Dual-wavelength rectangular pulse erbium-doped fiber laser based on topological insulator saturable absorber

Bo Guo,[1,*] Yong Yao,[1,4] Yan-Fu Yang,[1] Yi-Jun Yuan,[1] Lei Jin,[2] Bo Yan,[3] and Jian-Yu Zhang[1]

[1]*School of Electronic and Information Engineering, Shenzhen Graduate School, Harbin Institute of Technology, Shenzhen 518055, China*
[2]*School of Materials Science and Engineering, Shenzhen Graduate School, Harbin Institute of Technology, Shenzhen 518055, China*
[3]*College of Materials Science and Engineering, Zhengzhou University, Zhengzhou 450052, China*
[4]*e-mail: yaoyong@hit.edu.cn*
**Corresponding author: guobo512@163.com*

Received January 6, 2015; revised February 28, 2015; accepted March 1, 2015; posted March 2, 2015 (Doc. ID 231779); published April 17, 2015

We reported on the generation of the dual-wavelength rectangular pulse in an erbium-doped fiber laser (EDFL) with a topological insulator saturable absorber. The rectangular pulse could be stably initiated with pulse width from 13.62 to 25.16 ns and fundamental repetition rate of 3.54 MHz by properly adjusting the pump power and the polarization state. In addition, we verified that the pulse shape of the dual-wavelength rectangular pulse can be affected by the total net cavity dispersion in the fiber laser. Furthermore, by properly rotating the polarization controllers, the harmonic mode-locking operation of the dual-wavelength rectangular pulse was also obtained. The dual-wavelength rectangular pulse EDFL would benefit some potential applications, such as spectroscopy, biomedicine, and sensing research.

OCIS codes: (140.4050) Mode-locked lasers; (190.4370) Nonlinear optics, fibers; (160.4330) Nonlinear optical materials.
http://dx.doi.org/10.1364/PRJ.3.000094

1. INTRODUCTION

Rectangular pulse fiber lasers are of great importance due to their versatile applications in optical communication, spectroscopy, sensing research, laser micromachining, and ablation [1]. In 1992, Matsas *et al.* firstly observed the rectangular pulse in fiber laser with anomalous dispersion regime [2]. Since then, several actively/passively mode-locked techniques have been exploited for achieving rectangular pulse in fiber lasers. Compared with active scheme [3], passive schemes share more benefits: (1) very simple, compact, and low-cost without a modulator required; and (2) easily achieving rectangular pulses with ultrahigh peak power. To date, several passive mode-locking techniques, such as nonlinear polarization rotation (NPR) [4–9], nonlinear amplifying loop mirror [10], saturable absorber {SA, e.g., graphene oxide (GO) [11]}, and even hybrid NPR and active mode-locking [12] have been used to generate the rectangular pulse in the fiber lasers. Among them, SA-based mode-locker is thought to be more promising and efficient. To understand the operation and propagation mechanism of the square pulse, nonlinear polarization switching and dissipative soliton resonance (DSR) have been proposed and verified in [2,6–9], respectively. Notably, the generation of the rectangular pulse mentioned previously refers to only single-wavelength operation. Interestingly, Lin *et al.* observed the dual-wavelength domain-wall rectangular-shape pulse in a highly nonlinear fiber-based fiber ring laser [13]. Thus, properly increasing highly nonlinear effect in the laser cavity is favorable for generating multi-wavelength pulse. In addition, we also verified it in our recent work [14]. Furthermore, Zhao *et al.* reported on the generation of dual-wavelength rectangular pulse in a Yb-doped fiber laser by using a microfiber-based graphene saturable absorber (GSA) [15]. They demonstrated that the dual-wavelength mode-locked rectangular pulse could be regarded as DSR pulse. Taking into account the important applications of the multi-wavelength pulsed fiber laser [13–20], it would be interesting to know whether the multi-wavelength rectangular pulse could be explored by the new method.

Recently, a rising two-dimensional (2D) layer-by-layer material: topological insulators (TIs), characterized by a robust metallic edge or surface state and a narrow band-gap bulk topological insulating state, have gained great scientific and technical attention in physics, chemistry, and materials fields [21]. In 2012, Bernard *et al.* highlighted that a TI exhibits SA-like behavior when placed in a 1550 nm laser beam [22]. Since then, TIs including Bi_2Te_3, Bi_2Se_3, and Sb_2Te_3 have been found to be other perfect and efficient SAs for mode-locked [23–30] or *Q*-switched [31–35] fiber lasers at different wavelengths 1064, 1550, 1645, and 1935 nm due to their excellent wideband saturable absorption performance. Among these TIs, Bi_2Se_3 has a relatively larger bulk band gap (~0.3 eV) and is considered as a promising optical material for room-temperature applications [35]. Interestingly, in addition to the saturable absorption effect, Lu *et al.* also revealed that the TI:Bi_2Se_3 film shows a giant third-order optical nonlinear refractive index with a value of 10^{-14} m^2 W^{-1}, which is

comparable to graphene (10^{-12} m^2 W^{-1}) and much larger than carbon nanotubes (10^{-17} m^2 W^{-1}) [36]. Thus, the TIs could serve as both the high nonlinear photonic device and the SA in the laser system, which facilitates optical nonlinear phenomena, such as harmonic mode-locking (HML) [24], multi-soliton [25] and bright-dark soliton pair [30]. Notably, the fiber lasers with high nonlinearity were found to be more favorable for generating multi-wavelength pulses [13–15]. However, TI-assisted fiber laser with rectangular pulse has not yet been reported so far, to the best our knowledge.

In this paper, we demonstrate the dual-wavelength rectangular pulse in an erbium-doped fiber laser (EDFL) with a TI SA could be stably initiated with pulse width from 13.62 to 25.16 ns and fundamental repetition rate of 3.54 MHz by properly adjusting the pump power and the polarization state. In addition, we verified that the pulse shape of the dual-wavelength rectangular pulse could be affected by the total net cavity dispersion in the fiber laser. Furthermore, by properly rotating the polarization controllers (PCs), the HML operation of the dual-wavelength rectangular pulse was also obtained. This work demonstrates an example of the simultaneous applications of excellent saturable absorption and highly nonlinear effect of TI for rectangular-pulse EDFL.

2. PREPARATION AND OPTICAL PERFORMANCE OF TI SA

The few-layer TI:Bi_2Se_3 could be synthesized by several methods such as molecular beam epitaxial growth, chemical vapor–liquid–solid growth, and mechanical exfoliation by Scotch tape or peeling by an atomic force microscope tip from bulk crystals [28]. In this work, the TI:Bi_2Se_3/polyvinyl alcohol (PVA) film used in our work was synthesized via a solution-phase exfoliation/spin-coating method [35]. Initially, the bulk Bi_2Se_3 powders were added into the chitosan acetic solution solvents. After sonication for 30 h, the exfoliated Bi_2Se_3 was well-dispersed in these solvents. Then, the TI acetone solution was mixed with aqueous solution of PVA and ultrasonicated for 30 min. The mixture is then evaporated in an oven on a glass slide to obtain a TI:Bi_2Se_3/PVA film.

Before transferring the TI film into the fiber laser, we characterized this TI:Bi_2Se_3/PVA film as follows. First, its thickness (~25 μm) was measured with an alpha-step profiler (Surface Profiler P-10). Second, its morphological property was investigated with scanning electron microscopy (SEM) using Auriga Cross-Beam Workstation. The SEM images in Figs. 1(a) and 1(b) show that the TI film exhibits sheet-like structure with different resolution. Third, its microstructure was characterized by Raman spectroscopy at 514 nm wavelength of an argon–ion laser. Notably, in order to verify whether the physical performance of the few-layer Bi_2Se_3 nanosheets was affected by PVA, we measured the Raman spectrum of the TI:Bi_2Se_3/PVA film and the TI:Bi_2Se_3. Figure 1(c) shows the spectrum of the TI–PVA film, which shows the Raman peaks of both TI Bi_2Se_3 and PVA. Figure 1(d) presents three typical Raman peaks of Bi_2Se_3 centered at ~71.2 , ~130 , and ~171.6 cm^{-1}, which correspond to the out-of-plane vibrational mode A_{1g}^1, in-plane vibrational mode E_g^2, and the out-of-plane vibrational mode A_{1g}^2 of Se–Bi–Se–Bi–Se lattice vibration, respectively. Clearly, this Raman spectrum is consistent with the previously reported one [28]. Therefore, we can conclude that the few-layer Bi_2Se_3 could still keep their structures even though they are embedded into PVA matrix.

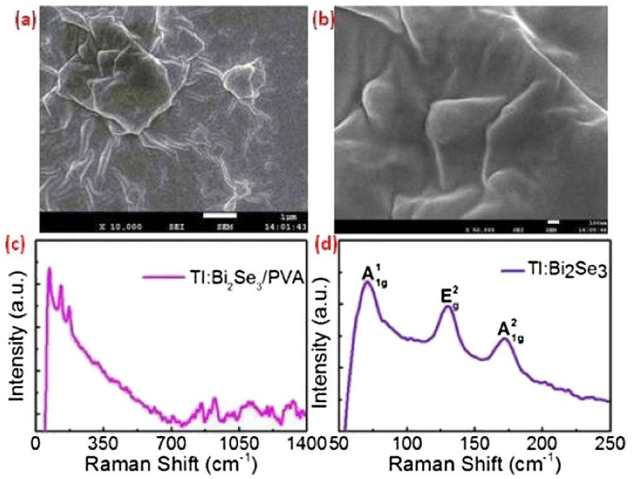

Fig. 1. (a) SEM images of the TI:Bi_2Se_3/PVA film with a resolution of 1 μm; (b) SEM images of the TI:Bi_2Se_3/PVA film with a resolution of 100 nm; (c) Raman spectrum of the TI:Bi_2Se_3/PVA film; (d) Raman spectrum of the TI:Bi_2Se_3 nanosheets.

We then experimentally investigated the nonlinear optical characteristics of the fabricated TI:Bi_2Se_3/PVA film by using the power-dependent transmission technique. The experimental setup used is similar with that in [24]. When the TI sample was illuminated by a femtosecond Ti:sapphire laser with a pulse width of 100 fs, we obtained its nonlinear absorption curve, as shown in Fig. 2. It shows a modulation depth (δT = 4.1%) and the saturable optical intensity (I_{SA} = 26 MW/cm^2), which is comparable to previous reports [14,28]. With such low saturable intensity, one can predict that the threshold of mode-locking operation can be significantly reduced. In addition, we also measured the optical inserting loss (~3 dB) of the TI SA by a power meter. Notably, the relatively low cavity loss is a very important index for improving multi-wavelength and mode-locking in the fiber laser, according to previous work [14,18].

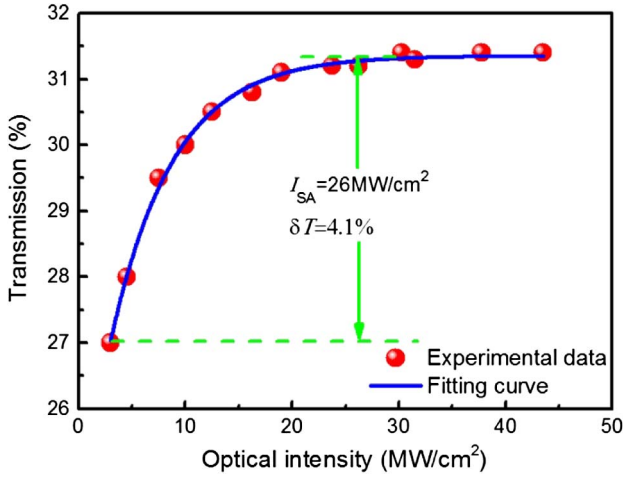

Fig. 2. Nonlinear saturable absorption curve of the TI:Bi_2Se_3/PVA film.

3. EXPERIMENTAL SETUP

The experimental setup of the proposed fiber laser is sketched in Fig. 3. The laser cavity consists of a piece of ~4.5 m highly doped erbium-doped fiber (Core active L900,) with dispersion parameter of approximately −16.3 ps/(km · nm), peak absorption of 14.5 dB/m at 1530 nm, and ~53 m single-mode fiber (SMF) with dispersion parameter of 18 ps/(km · nm). The total net cavity dispersion is approximately −1.1 ps^2. A fiber-pigtailed 974 nm laser diode (LD; 980-200-B-FA) with maximum power ~200 mW via a fused 980/1550 wavelength-division multiplexer (WDM) is used to pump source and a 10:90 optical coupler (OC) is employed to extract the output of the laser beam. A polarization-independent isolator (ISO) and a PC were used to force the unidirectional operation of the ring cavity and adjust the polarization state of the propagation light, respectively. The optical performance of the laser was monitored by a power meter, an optical spectrum analyzer (ANDO AQ-6317B) with spectral resolution of 0.01 nm and a photo-detector (PDA 2GHz) combined with a 1 GHz mixed oscilloscope (MDO4054-6, 5 GHz/s), respectively.

4. RESULTS AND DISCUSSION

First, we verified the operation characteristic of the fiber laser without incorporating the TI SA. By adjusting the pump strength and the cavity polarization state in a wide range, there is neither mode-locking nor dual-wavelength generation, which exclude the possibility of self-mode-locking and the Fabry–Perot cavity effect in the cavity. Then, a small piece of sample (~1 mm × 1 mm), which is cut from the TI/PVA film, is sandwiched by two fiber connectors to form a fiber-compatible mode-locker. Thereafter, a series of experiments show that the stable dual-wavelength rectangular pulse can be easily obtained by properly rotating the PC.

In this paper, we concentrate our discussion on the dual-wavelength rectangular pulse performance at the pump power of 90 mW in our proposed fiber laser. By properly adjusting the PC, the optical spectrum of the dual-wavelength rectangular pulse is given in Fig. 4(a). It contains two wavelengths, centered at 1561.6 and 1562.1 nm, with the same 3 dB bandwidth of 0.25 nm. The intensity difference between the spectral peak and valley is about 3 dB. The typical pulse train of the laser output, depicted in Fig. 4(b), has a period of 282.4 ns, which matches with the cavity roundtrip time and verifies

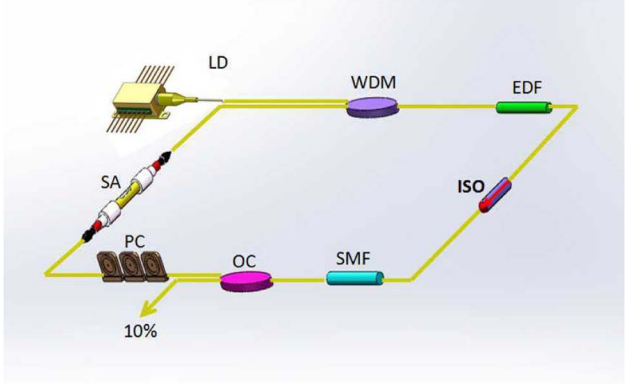

Fig. 3. Experimental setup of dual-wavelength rectangular pulses fiber laser with a TI SA. EDF, erbium-doped fiber.

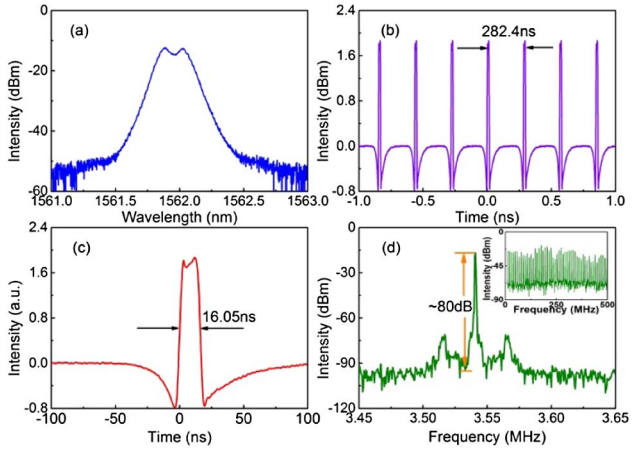

Fig. 4. Typical dual-wavelength rectangular pulse characteristics at the pump power of 90 mW; (a) output optical spectrum; (b) pulse train; (c) zoom-in single-pulse profile; (d) RF spectrum (inset, RF spectrum measured in 500 MHz range).

the mode-locking state. In addition, no fine structure can be observed by using a high bandwidth photodetector. Figure 4(c) shows a zoom-in single-pulse profile. The pulse has a rectangular intensity profile with a full width at half-maximum (FWHM) of 16.05 ns. As we know, due to the slow response time of the photodetector and sampling oscilloscope, the single oscilloscope trace could not reflect the real pulse shape for the ultrafast pulses. Thereafter, a commercial optical auto-correlator (FR-103MN) was used to check the fine structure of the dual-wavelength rectangular pulse. Surprisingly, no pulse signal could be detected; this may be because the nanosecond duration of the rectangular pulse is beyond the maximum measurement range of the autocorrelator, which verifies that the rectangular pulse is not the combination of multi-soliton [25]. To investigate the stability of the dual-wavelength rectangular pulse, we measured its radio frequency (RF) spectrum, as shown in Fig. 4(d). Its fundamental peak, located at the cavity repetition rate of 3.54 MHz, has a signal-to-noise ratio of ~80 dB, indicating relative good stability and further confirming its mode-locking operation. Notably, similar to our previous work [14,30], we can see that two small sidebands are presented due to the dual-wavelength operation. In addition, the operation stability of the proposed dual-wavelength rectangular pulse EDFL may be affected by the cavity loss and the quality of the TI:Bi_2Se_3/PVA film. Furthermore, we also provide the RF spectrum in a larger range (500 MHz). As shown in the inset of Fig. 4(d), the rectangular pulse exhibits relatively good mode-locking stability.

Then the pump-dependent evolutions of the dual-wavelength rectangular pulse were investigated and are shown in Fig. 5, where self-started mode-locking and dual-wavelength rectangular pulse occur when pump power exceeds 20 and 80 mW, respectively. For pump power below 80 mW, no dual-wavelength rectangular pulse appears and only single-wavelength is presented. As we know, the combination of the intra-cavity birefringence of the SMF and the polarization-dependent loss of the PC which could induce a comb filtering effect facilitates the dual-wavelength operation. Benefiting from the both excellent saturable absorption and high nonlinearity of TI:Bi_2Se_3, it is naturally expected that

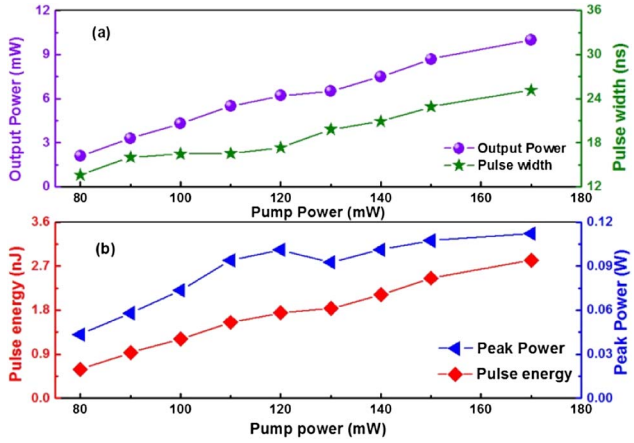

Fig. 5. (a) Output average power and pulse width; (b) pulse energy and peak power of rectangular pulse versus incident pump power.

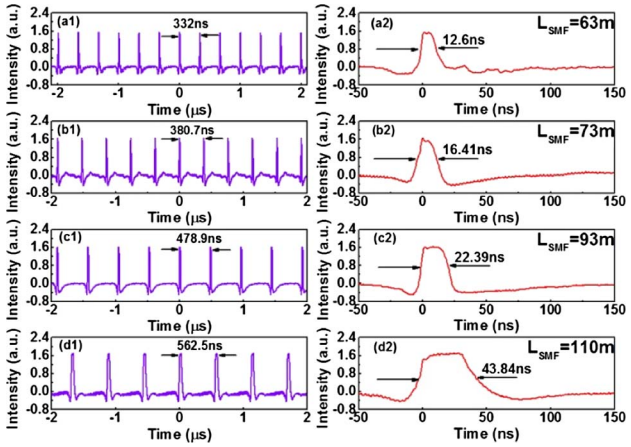

Fig. 6. Typical time-domain characteristics of the rectangular pulse with different length of the SMF. Pulse train and corresponding single pulse profile of the rectangular pulse when (a) $L_{SMF} = 63$ m, $\beta_{2,cavity}$ = approximately – 1.34 ps^2; (b) $L_{SMF} = 73$ m, $\beta_{2,cavity}$ = approximately –1.57 ps^2; (c) $L_{SMF} = 93$ m, $\beta_{2,cavity}$ = approximately – 2.03 ps^2; (d) $L_{SMF} = 110$ m, $\beta_{2,cavity}$ = approximately – 2.42 ps^2.

dual-wavelength rectangular pulse could be achieved by properly adjusting the pump power and the polarization state. Figure 5(a) shows the measured pulse width and the average output power versus the pump power. Clearly, the pulse width and output power of dual-wavelength rectangular pulse increase monotonically from 13.62 to 25.16 ns and from 2.1 to 10 mW, respectively, as the pump power increased from 80 to 170 mW. Furthermore, we present the pulse energy and peak power of dual-wavelength rectangular pulse versus the pump power. As shown in Fig. 5(b), its pulse energy and peak power increase also monotonically from 0.593 to 2.824 nJ and from 43.6 to 112 mW, respectively, when the pump power increased from 80 to 170 mW. Similarly to previous work [7,8], the pulse width and peak power of the rectangular pulse increase approximately linearly in accordance with pumping strength. Thus, we believe the rectangular pulse could be also regarded as the DSR pulse.

Clearly, for the dual-wavelength rectangular pulse in Fig. 4(c), its pulse profile deviated from that of the common DSR pulse, implying that its dynamics may be affected by the cavity dispersion, according to the dispersion theory in [1]. Next, we consider the effect of the total net anomalous cavity dispersion ($\beta_{2,cavity}$) on the pulse profile of the dual-wavelength rectangular pulse by only adjusting the length of the SMF (L_{SMF}) in our proposed laser cavity. To this end, by gradually lengthening L_{SMF} from ~63 to ~110 m, we can see that the pulse width of the dual-wavelength rectangular pulse broadens, as shown in Fig. 6. In addition, in accordance with a larger $\beta_{2,cavity}$, the shape of the rectangular pulse becomes more smooth. Thus, we believe that the total net cavity dispersion has an important effect on the formation and dynamics of the dual-wavelength rectangular pulse. Meanwhile, we notice that the pulse amplitude was almost clamped at a constant level during the pulse broadening, which further verifies the rectangular pulse belongs to the DSR pulse, according to the previous work [9,10]. Notably, we obtain a relatively good rectangular pulse when L_{SMF} is about 93 m, as shown in Fig. 6(c). We hope the performance of the dual-wavelength rectangular pulse will be further improved by optimizing the design of the laser cavity and improving the quality of the TI:Bi_2Se_3/PVA film in our future work.

Distinct from previous work [3–10], that is, the mode-locked pulse operating in DSR regime is wave-breaking-free. Surprisingly, we observed the HML of the dual-wavelength rectangular pulse in experiments. As shown in Fig. 7, we obtain its first, second, third, and fifth HML operation by properly adjusting the pump power and the polarization state. To understand the HML operation of the dual-wavelength rectangular pulse, we should consider that the splitting of solitons in the cavity is related to the pump power and the high accumulated nonlinearity. According to previous work [14,36], TI:Bi_2Se_3 shows very high nonlinearity. Thus, the single DS circulating in the cavity can be split into multiple DSs at higher pump power levels due to the interplay between the laser cavity bandwidth constraints and the energy quantization effect [1]. In such regime, these DSs are usually randomly located in the cavity. However, they can automatically arrange themselves and equally locate in the laser cavity forming the HML state by properly adjusting the pump power and the polarization state. In addition, we also notice that Lin *et al.* observed the HML of square pulse in a passively mode-locked Yb-doped fiber laser based on a GO SA [11].

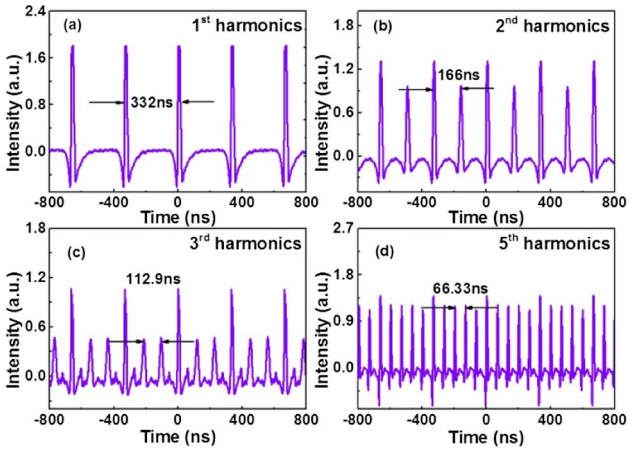

Fig. 7. Oscilloscope traces of first, second, third, and fifth HML of the dual-wavelength rectangular pulse when properly adjusting the pump power and the polarization state.

To understand why the dual-wavelength rectangular pulse could be formed in our laser, we notice that Zhao *et al.* demonstrated the dual-wavelength rectangular pulse from an Yb-doped fiber laser with a GSA could be regarded as DSR pulse [15]. Notably, besides rectangular pulse, we also observed the dual-wavelength step-like pulse in the work, which is similar to the previous report [37]. Distinct from the rectangular pulse, it exhibits two-level step-like profiles. Inspired by previous work, we believe our dual-wavelength rectangular pulse could be resolved as two independent rectangular pulses. The detailed formation and propagation mechanism of the rectangular pulse will be well-discussed in future research.

Finally, we tested the damage threshold of the TI SA (~200 mW) in our work. Interestingly, we also notice that other 2D materials, such as MoS_2 [38] and WS_2 [39,40] were demonstrated to be good candidates of the highly nonlinear photonic device in fiber lasers. We hope the rectangular pulse could be observed by them in future research.

5. CONCLUSION

In conclusion, we have proposed and demonstrated the generation of dual-wavelength rectangular pulses in an EDFL with a TI SA. The rectangular pulse could be stably initiated with pulse width from 13.62 to 25.16 ns and fundamental repetition rate of 3.54 MHz by properly adjusting the pump power and the polarization state. In addition, we verified that the pulse shape of the dual-wavelength rectangular pulse can be affected by the total net cavity dispersion in the fiber laser. Moreover, by properly rotating the PCs, the HML operation of the dual-wavelength rectangular pulse was also obtained. Our experiment verifies that the TIs show both excellent saturable absorption and high nonlinearity simultaneously. We hope this kind of dual-wavelength rectangular pulse fiber laser at 1.5 μm will find some potential applications in spectroscopy, biomedicine, and sensing research.

ACKNOWLEDGMENTS

The authors acknowledge Professor Z. Q. Luo (Xiamen University, China) and H. Zhang (Shenzhen University, China) for supporting the TI sample and also acknowledge the Professors D. Mao (Northwestern Poly-Technical University, China) and Z. C. Luo (South China Normal University, China) for helpful discussions. The SEM image was obtained at the Shenzhen Key Laboratory of Advanced Materials Lab, Harbin Institute of Technology. This work was supported by National Natural Science Foundation of China (No. 612050346) and the Shenzhen Municipal Science and Technology Plan (Nos. 2010B090400306, JC201105160592A, and JCYJ 20120613150130014).

REFERENCES

1. G. P. Agrawal, *Nonlinear Fiber Optics*, 5th ed. (Academic, 2013).
2. V. J. Matsas, T. P. Newson, and M. N. Zervas, "Self-starting passively mode-locked fibre ring laser exploiting nonlinear polarisation switching," Opt. Commun. **92**, 61–66 (1992).
3. H. Chen, S. P. Chen, Z. F. Jiang, and J. Hou, "Flexible rectangular wave-breaking-free pulse generation in actively mode-locked ytterbium-doped fiber laser," Opt. Express **22**, 26449–26456 (2014).
4. X. Li, X. Liu, X. Hu, L. Wang, H. Lu, Y. Wang, and W. Zhao, "Long-cavity passively mode-locked fiber ring laser with high-energy rectangular-shape pulses in anomalous dispersion regime," Opt. Lett. **35**, 3249–3251 (2010).
5. D. Mao, X. Liu, L. Wang, H. Lu, and H. Feng, "Generation and amplification of high-energy nanosecond pulses in a compact all-fiber laser," Opt. Express **18**, 23024–23029 (2010).
6. X. Wu, D. Y. Tang, H. Zhang, and L. M. Zhao, "Dissipative soliton resonance in an all-normal-dispersion erbium-doped fiber laser," Opt. Express **17**, 5580–5584 (2009).
7. Z. C. Luo, W. J. Cao, Z. B. Lin, Z. R. Cai, A. P. Luo, and W. C. Xu, "Pulse dynamics of dissipative soliton resonance with large duration-tuning range in a fiber ring laser," Opt. Lett. **37**, 4777–4779 (2012).
8. L. Duan, X. Liu, D. Mao, L. Wang, and G. Wang, "Experimental observation of dissipative soliton resonance in an anomalous-dispersion fiber laser," Opt. Express **20**, 265–270 (2012).
9. L. Liu, J. H. Liao, Q. Y. Ning, W. Yu, A. P. Luo, S. H. Xu, Z. C. Luo, Z. M. Yang, and W. C. Xu, "Wave-breaking-free pulse in an all-fiber normal-dispersion Yb-doped fiber laser under dissipative soliton resonance condition," Opt. Express **21**, 27087–27092 (2013).
10. H. Lin, C. Guo, S. Ruan, and J. Yang, "Dissipative soliton resonance in an all-normal-dispersion Yb-doped figure-eight fibre laser with tunable output," Laser Phys. Lett. **11**, 085102 (2014).
11. R. Y. Lin, Y. G. Wang, P. G. Yan, G. L. Zhang, J. Q. Zhao, H. Q. Li, and J. A. Duan, "Bright and dark square pulses generated from a graphene-oxide mode-locked ytterbium-doped fiber laser," IEEE Photon. J. **6**, 1–8 (2014).
12. X. Fang, P. K. Wai, C. Lu, H. Y. Tam, and S. H. Wang, "Flat-top pulse generation based on the combined action of active mode locking and nonlinear polarization rotation," in *Conference on Lasers and Electro-Optics* (Optical Society of America, 2008), paper JTuA91.
13. Z. B. Lin, A. P. Luo, S. K. Wang, H. Y. Wang, W. J. Cao, Z. C. Luo, and W. C. Xu, "Generation of dual-wavelength domain-wall rectangular-shape pulses in HNLF-based fiber ring laser," Opt. Laser Technol. **44**, 2260–2264 (2012).
14. B. Guo, Y. Yao, Y. F. Yang, Y. J. Yuan, R. L. Wang, S. G. Wang, Z. H. Ren, and B. Yan, "Topological insulator: Bi_2Se_3/polyvinyl alcohol film-assisted multi-wavelength ultrafast erbium-doped fiber laser," J. Appl. Phys. **117**, 063108 (2015).
15. N. Zhao, M. Liu, H. Liu, X. W. Zheng, Q. Y. Ning, A. P. Luo, Z. C. Luo, and W. C. Xu, "Dual-wavelength rectangular pulse Yb-doped fiber laser using a microfiber-based graphene saturable absorber," Opt. Express **22**, 10906–10913 (2014).
16. H. Zhang, D. Y. Tang, X. Wu, and L. M. Zhao, "Multi-wavelength dissipative soliton operation of an erbium-doped fiber laser," Opt. Express **17**, 12692–12697 (2009).
17. Z. X. Zhang, Z. W. Xu, and L. Zhang, "Tunable and switchable dual-wavelength dissipative soliton generation in an all-normal-dispersion Yb-doped fiber laser with birefringence fiber filter," Opt. Express **20**, 26736–26742 (2012).
18. Z. Luo, M. Zhou, Z. Cai, C. Ye, J. Weng, G. Huang, and H. Xu, "Graphene-assisted multiwavelength erbium-doped fiber ring laser," IEEE Photon. Technol. Lett. **23**, 501–503 (2011).
19. X. Liu, D. Han, Z. Sun, C. Zeng, H. Lu, D. Mao, Y. Cui, and F. Wang, "Versatile multi-wavelength ultrafast fiber laser mode-locked by carbon nanotubes," Sci. Rep. **3**, 2718 (2013).
20. Z. Chen, H. Sun, and S. Ma, "Dual-wavelength mode-locked erbium-doped fiber ring laser using highly nonlinear fiber," IEEE Photon. Technol. Lett. **20**, 2066–2068 (2008).
21. X. L. Qi and S. C. Zhang, "Topological insulators and superconductors," Rev. Mod. Phys. **83**, 1057–1110 (2011).
22. F. Bernard, H. Zhang, S. P. Gorza, and P. Emplit, "Towards mode-locked fiber laser using topological insulators," in *Nonlinear Photonics* (OSA, 2012), paper NTh1A.5.
23. C. Zhao, H. Zhang, X. Qi, Y. Chen, Z. Wang, S. Wen, and D. Tang, "Ultra-short pulse generation by a topological insulator based saturable absorber," Appl. Phys. Lett. **101**, 211106 (2012).
24. Z. C. Luo, M. Liu, H. Liu, X. W. Zheng, A. P. Luo, C. J. Zhao, H. Zhang, S. C. Wen, and W. C. Xu, "2 GHz passively harmonic mode-locked fiber laser by a microfiber-based topological insulator saturable absorber," Opt. Lett. **38**, 5212–5215 (2013).
25. Y. Chen, M. Wu, P. Tang, S. Chen, J. Du, G. Jiang, and S. Wen, "The formation of various multi-soliton patterns and noise-like pulse in a fiber laser passively mode-locked by a topological

insulator based saturable absorber," Laser Phys. Lett. **11**, 055101 (2014).
26. M. Jung, J. Lee, J. Koo, J. Park, Y. W. Song, K. Lee, S. Lee, and J. H. Lee, "A femtosecond pulse fiber laser at 1935 nm using a bulk-structured Bi_2Te_3 topological insulator," Opt. Express **22**, 7865–7874 (2014).
27. J. Sotor, G. Sobon, W. Macherzynski, P. Paletko, K. Grodecki, and K. M. Abramski, "Mode-locking in Er-doped fiber laser based on mechanically exfoliated Sb_2Te_3 saturable absorber," Opt. Mater. Express **4**, 1–6 (2014).
28. H. Liu, X. W. Zheng, M. Liu, N. Zhao, A. P. Luo, Z. C. Luo, and S. C. Wen, "Femtosecond pulse generation from a topological insulator mode-locked fiber laser," Opt. Express **22**, 6868–6873 (2014).
29. P. Yan, R. Lin, S. Ruan, A. Liu, and H. Chen, "A 2.95 GHz, femtosecond passive harmonic mode-locked fiber laser based on evanescent field interaction with topological insulator film," Opt. Express **23**, 154–164 (2015).
30. B. Guo, Y. Yao, J. Tian, Y. Zhao, S. Liu, M. Li, and M. Quan, "Observation of bright-dark soliton pair in a mode-locked fiber laser with topological insulator," IEEE Photon. Technol. Lett. **27**, 701–704 (2015).
31. Y. Chen, C. Zhao, S. Chen, J. Du, P. Tang, G. Jiang, H. Zhang, S. Wen, and D. Tang, "Large energy, wavelength widely tunable, topological insulator *Q*-switched erbium-doped fiber laser," IEEE J. Sel. Top. Quantum Electron. **20**, 315–322 (2014).
32. Z. Yu, Y. Song, J. Tian, Z. Dou, H. Yang, G. Yu, K. Li, H. Li, and X. Zhang, "High-repetition-rate *Q*-switched fiber laser with high quality topological insulator Bi_2Se_3 film," Opt. Express **22**, 11508–11515 (2014).
33. Z. Luo, C. Liu, Y. Huang, D. Wu, J. Wu, H. Xu, Z. Cai, Z. Lin, L. Sun, and J. Wen, "Topological-insulator passively *Q*-switched double-clad fiber laser at 2 μm wavelength," IEEE J. Sel. Top. Quantum Electron. **20**, 0902708 (2014).
34. Z. Luo, Y. Huang, J. Weng, H. Cheng, Z. Lin, B. Xu, Z. Cai, and H. Xu, "1.06 μm *Q*-switched ytterbium-doped fiber laser using few-layer topological insulator Bi_2Se_3 as a saturable absorber," Opt. Express **21**, 29516–29522 (2013).
35. L. Sun, Z. Lin, J. Peng, J. Weng, Y. Huang, and Z. Luo, "Preparation of few-layer bismuth selenide by liquid-phase-exfoliation and its optical absorption properties," Sci. Rep. **4**, 4794–4802 (2014).
36. S. Lu, C. Zhao, Y. Zou, S. Chen, Y. Chen, Y. Li, H. Zhang, S. Wen, and D. Tang, "Third order nonlinear optical property of Bi_2Se_3," Opt. Express **21**, 2072–2082 (2013).
37. D. Mao, X. Liu, L. Wang, H. Lu, and L. Duan, "Dual-wavelength step-like pulses in an ultra-large negative-dispersion fiber laser," Opt. Express **19**, 3996–4001 (2011).
38. M. Liu, X. W. Zheng, Y. L. Qi, H. Liu, A. P. Luo, Z. C. Luo, W. C. Xu, C. J. Zhao, and H. Zhang, "Microfiber-based few-layer MoS_2 saturable absorber for 2.5 GHz passively harmonic mode-locked fiber laser," Opt. Express **22**, 22841–22846 (2014).
39. P. Yan, A. Liu, Y. Chen, H. Chen, S. Ruan, C. Guo, S. Chen, I. L. Li, H. Yang, J. Hu, and G. Cao, "Microfiber-based WS_2-film saturable absorber for ultra-fast photonics," Opt. Mater. Express **5**, 479–489 (2015).
40. D. Mao, Y. Wang, C. Ma, L. Han, B. Jiang, X. Gan, S. Hua, W. Zhang, T. Mei, and J. Zhao, "WS_2 mode-locked ultrafast fiber laser," Sci. Rep. **5**, 7965 (2015).